International Journal of Biological Macromolecules 180 (2021) 212–221

Contents lists available at ScienceDirect

International Journal of Biological Macromolecules

journal homepage: http://www.elsevier.com/locate/ijbiomac

Electrospun lignin-PVP nanofibers and their ability for structuring oil

María Borrego, José E. Martín-Alfonso, M. Carmen Sánchez, Concepción Valencia, José M. Franco *

Pro²TecS – Chemical Product and Process Technology Research Center, Department of Chemical Engineering and Materials Science, Universidad de Huelva, ETSI, Campus de "El Carmen", 21071 Huelva, Spain

ARTICLE INFO

Article history:
Received 9 February 2021
Received in revised form 4 March 2021
Accepted 12 March 2021
Available online 16 March 2021

Keywords:
Electrospinning
Lignin
Nanofiber
Oil structuring
Oleogel
Rheology

ABSTRACT

This work explores the electrospinnability of low-sulfonate Kraft lignin (LSL)/polyvinylpyrrolidone (PVP) solutions in *N*,*N*-dimethylformamide (DMF) and the ability of the different micro- and nano-architectures generated to structure castor oil. LSL/PVP solutions were prepared at different concentrations (8–15 wt%) and LSL:PVP ratios (90:10–0:100) and physico-chemically and rheologically characterized. The morphology of electrospun nanostructures mainly depends on the rheological properties of the solution. Electrosprayed nanoparticles or micro-sized particles connected by thin filaments were obtained from solutions with low LSL/PVP concentrations and/or high LSL:PVP ratios, whereas beaded or bead-free nanofibers were produced by increasing concentration and/or decreasing LSL:PVP ratio, due to enhanced extensional viscoelastic properties and non-Newtonian characteristics. Electrospun LSL/PVP nanofibers are able to form oleogels by simply dispersing them into castor oil at concentrations between 10 and 30 wt%. The rheological properties of the oleogels may be tailored by modifying the LSL:PVP ratio and nanofibers content. The potential application of these oleogels as bio-based lubricants was also explored in a tribological cell. Satisfactory friction and wear results are achieved when using oleogels structured by nanofibers mats with enhanced gel-like properties as lubricants. Overall, electrospinning of lignin/PVP solutions can be proposed as a simple and effective method to produce nanofibers for oil structuring.

1. Introduction

As has been collected in recent reviews [1–5], oleogelation and oil structuring have attracted a great deal of interest in the research community over the last decade, especially in food applications but also in the field of pharmaceuticals [6–8] and lubricants [9–11]. In particular, in the lubricant industry, the development of oleogelators and oil thickeners from natural polymers, making them technologically efficient, represents a major challenge in terms of environmentally friendly alternatives to synthetic polymers derived from the petrochemical industry or metal soap-based thickeners, which are either not biodegradable or require highly toxic production processes. Unfortunately, only a few biopolymers are able to gel oils directly by formation of supramolecular structures through physical entanglements or chemical crosslinking among polymer chains [12], which must balance solvent-gelator and gelator-gelator interactions [2]. Among these biopolymers, ethylcellulose is the most widely used for different applications [13–16]. Besides, other indirect pathways to gel oils using hydrophilic biopolymers have been proposed, such as the so-called foam-templated [17] and emulsion-templated [18,19] approaches or stepwise solvent-exchange routes [20,21], resulting in porous structures where oil can be adsorbed or entrapped. Nonetheless, in most cases, these strategies are highly time-, solvent- and/or energy-consuming. Another alternative approach is the chemical modification of the biopolymers to increase the compatibility with oil media thus favouring oleogelation. Oil structuring can be achieved physically, by reducing the polymer polarity, thus modifying the solvent-biopolymer hydrophobic interactions, for example by inserting methyl, ethyl or acyl groups into their structure, or chemically, by functionalization with reactive groups able to produce covalent interactions with the oil, thus promoting a certain degree of cross-linking between the medium and the biopolymer. These routes have been widely reported to produce oleogels and stable gel-like dispersions using different lignocellulosic materials and cellulose or chitosan derivatives [13,22–30]. Nevertheless, these chemical modifications may require chemicals, solvents and/or catalysts that make the process of oil structuring relatively complex and not completely environmentally friendly, even though the final product is.

Therefore, the search for new bio-sourced polymeric materials and the procedures for incorporating them into an oil matrix by promoting its structuration are still open research areas, particularly in the field of lubrication, which requires specific and rigorous technical performance, for example in terms of thermal and high shear resistance. To the best of our knowledge, biopolymer nanostructures generated by electrospinning or other similar techniques have not been evaluated as potential oil thickening or gelling agents. However, it can be hypothesized that the high porosity, small size and high surface/volume ratio of nanofibers may induce the formation of three-dimensional networks

* Corresponding author at: Departamento de Ingeniería Química, Universidad de Huelva, ETSI, Campus de "El Carmen", 21071 Huelva, Spain.
E-mail address: franco@uhu.es (J.M. Franco).

https://doi.org/10.1016/j.ijbiomac.2021.03.069
0141-8130/

with a great capacity to promote physical interactions between the oil and the nanofibers. In this sense, Muller et al. [31] attributed exceptional stabilizing effects and lubricant properties to the fact of using polypropylene nanoparticles suitably dispersed in a mineral oil, not only acting as an efficient oil structuring agent but also conferring other functional properties, i.e. reducing friction and wear in tribological contacts, improving mechanical stability or expanding the application temperature range.

Taking into account the biorefinery concept, conceived as a global industrial process capable of producing intermediate and end-use products from biomass in a versatile way [32], the interest in using lignocellulosic materials as raw materials in a wide variety of chemical and energy industries has been steadily increasing in recent years. To date, the potential of lignocellulosic biomass is mainly based on its carbohydrate content, particularly cellulose. Instead, the use and exploitation of lignin are much less explored, probably due to its complex chemical structure and the variability of its composition and structure depending on its source, among other factors. Despite this, lignin is considered a renewable resource with great potential for different industrial applications [33,34].

For the above mentioned reasons, the use of lignin to produce new oil structuring agents is justified as a new pathway of revalorization, which combines ecological, economic and social benefits. The main difficulty consists in selecting and developing an appropriate processing protocol and/or prior treatment of this particular biopolymer, which subsequently facilitate an efficient interaction with the oil. This study explores the use of the electrospinning technique as a tool to obtain lignin nanostructures which may be able to entrap oils generating oleogels directly, avoiding other stepwise procedures like those referred above. A vast number of studies have explored the possibility of obtaining nanofibers from a wide range of biopolymers or biodegradable synthetic polymers. For example, electrospun nanofibers of different polysaccharides, such as cellulose and chitosan, among others, were found to have great potential in different fields [35–37]. However, obtaining nanofibers from lignins by means of the electrospinning technique is still scarcely developed for different reasons. Among them, it is worth mentioning the heterogeneity of the chemical composition of lignins, their branched structure or the presence of low-molecular-weight compounds resulting from degradation during the biomass delignification process. These conditioning factors give rise to non-uniform structures consisting of particles or globules distributed along the filament, which has come to be called BOAS (beads on-a-string) [38]. Despite this, the production of lignin nanofibers by electrospinning is currently of increasing importance, due to the great potential of these nanostructured materials for several engineering applications, such as carbon fiber precursors, adsorbents, filters or medical implementations [39–41]. Notwithstanding, there is still much room for improvement, especially in terms of processability, which may cover the use of solvent mixtures, optimization of the rheological properties of the feed solution, doping with other polymers or prior chemical modification, among other options. Dallmeyer et al. [42] evaluated the electrospinability of seven different types of lignin solutions and, despite the various combinations tested, they did not obtain uniform nanofibers, but rather micro- or particulate nano-structures (BOAS). However, the addition of 1 wt% of polyethylene oxide (PEO) as a doping agent, produced lignin nanofibers with suitable morphology, depending on the concentration of the solution. The vast majority of the literature related to the formation of lignin nanofibers describes the use of other polymers to improve their electrospinability, such as PEO [38,43], polyvinyl acetate (PVA) [44,45], polyacrylonitrile and polyacrylamide [46], polyhydroxybutyrate (PHB) [47], polycaprolactone (PCL) [41,48], or polylactic acid (PLA) [40]. On the other hand, different solvents such as DMF, DMSO or hexafluoro-2-propanol (HFIP) have also been used in the above mentioned works, reflecting the importance of an adequate selection of the solvent and the rheological properties of the starting solution [38,49]. In this work, the electrospinability of low-sulfonate lignin solutions in DMF, doped with polyvinylpyrrolidone (PVP) at different ratios, was evaluated and the composite micro- and nanostructures generated were assessed as potential structuring agents for castor oil.

2. Materials and methods

2.1. Materials

Softwood low sulfonate Kraft lignin (LSL, Mw: ~10,000 g/mol) and polyvinylpyrrolidone (PVP, Mw: ~360,000 g/mol) were obtained from Merck Sigma-Aldrich. *N*,*N*-dimethyl formamide (DMF, purity ≥99,8%) was also acquired from Merck Sigma-Aldrich and used as solvent to prepared LSL/PVP solutions. Castor oil was supplied by Guinama (Spain). Fatty acid composition and main physical properties can be found elsewhere [50].

2.2. Solution preparation and characterization

LSL/PVP solutions in DMF were prepared to attain 8, 10 and 15 wt% total concentration, modifying the LSL:PVP ratio (90:10, 70:30, 50:50, 30:70, 10:90 and 0:100). First, the appropriated amount of PVP was weighed and dissolved in DMF by stirring for 2 h, at room temperature. Afterwards, the corresponding amount of LSL was added to the solution and left under agitation for 24 h at room temperature. Final solutions were centrifuged for 10 min at 3000 rpm and filtered to ensure that no undissolved solids were present.

LSL/PVP solutions were physico-chemically characterized through electrical conductivity, surface tension and shear and extensional viscosity measurements. Electrical conductivity was measured in a Laqua PC-110 conductivity meter using a 3553-10D LAQUA cell (Horiba Scientific). The conductivity cell was previously calibrated with standard KCl solutions of known conductivity (1413 μS/cm and 12.88 μS/cm, respectively). Measurements were replicated at least three times. Surface tension measurements were performed in a Sigma 703D tensiometer (Biolin Scientific) using a Wilhelmy platinum plate with a measuring range of 1–1000 mN/m. Measurements were made in duplicate at 20 °C. Shear viscometric measurements were performed, at 25 °C, in an ARES controlled-strain rheometer (Rheometric Scientific) using a Couette geometry (internal radius 16 mm, external radius 17 mm, cylinder length 33.35 mm), in a shear rate range 1–500 s^{-1}. At least two replicas of each of the test were performed. In those cases that LSL/PVP solutions exhibited a non-Newtonian response, data were satisfactorily fitted ($R^2 < 0.995$) to the Williamson model:

$$\eta = \frac{\eta_0}{1 + (K\,\dot{\gamma})^m} \tag{1}$$

where, η is the non-Newtonian viscosity, η_0 is the zero-shear-rate limiting viscosity; $\dot{\gamma}$ is the shear rate; m is a parameter related to the slope of the shear-thinning region and K is a constant whose inverse coincides with the shear rate for which $\eta = \eta_0/2$.

Extensional viscosity was evaluated by means of capillary breakup measurements using the CaBER-1 extensional rheometer (ThermoHaake). The filament was created by placing the solution sample between two parallel plates (6 mm diameter) and suddenly increasing the plate-plate separation from 1.5 to 15 mm in 10 ms. The extensional rheological properties were indirectly deduced from the evolution of the filament diameter with time, as extensively investigated and indicated elsewhere [51–53]. The apparent extensional viscosity can be quantified as:

$$\eta_{ext} = \frac{\sigma}{\left(-\frac{dD(t)}{dt}\right)} \tag{2}$$

where σ is the surface tension and D is the diameter of the filament.

2.3. Electrospinning

Electrospinning of LSL/PVP solutions was carried out in a Doxa Microfluids chamber using a vertical arrangement dealing with a 5 ml BD syringe of 11.99 mm internal diameter and a 20G flat-tip needle used as spinneret connected to the positive terminal of a high voltage source, whereas the negative terminal was connected to a flat aluminium plate collector arranged below the spinneret at a variable distance in which the LSL/PVP nanostructures were collected. The solution is pumped by a positive displacement pump under controlled flow. The electrospinning input parameters were modified according to the solution characteristics (see Table 1). A camera-monitor system coupled to the electrospinning chamber was used to visually verify the formation of the Taylor cone or detecting any agglomeration or flow instability in the needle tip (see Fig. 1), thus checking whether the set of electrospinning parameters is adequate or not. All experiments were carried out at room temperature (22 ± 1 °C) and relative humidity (53 ± 2%).

2.4. Characterization of LSL/PVP nanostructures

The morphology of LSL/PVP nanostructures was assessed by means of scanning electron microscopy (SEM) observations carried out in both JEOL, model JXA-8200 SuperProbe, and Hitachi, model FlexSEM 1000 II, microscopes, operating at 10–20 kV accelerating voltages and different magnifications. Samples were previously gold-coated using a sputter coater HHV Scancoat Six SEM.

A thermogravimetric analysis (TGA) was performed in a Q-50 balance (TA Instruments) under N_2 atmosphere. LSL/PVP nanostructures taken from the collector (5–10 mg) were placed on platinum pans and heated from 30 °C to 600 °C, at 10 °C min^{-1}.

2.5. Structuring castor oil with LSL/PVP nanostructures and rheological and tribological characterization

Castor oil was simply added slowly to the electrospun LSL/PVP nanostructures under gentle agitation at room conditions in the quantities needed to achieve final concentrations of LSL/PVP nanostructures of 10, 20 and 30 wt%. The homogeneity of the resulting dispersions was verified through observations in an Olympus BX51 optical microscope. Oleogels and/or structured dispersions were further rheologically characterized (at least 24 h after preparation) in a Rheoscope controlled-stress rheometer (TermoHaake, Germany) equipped with a thermostatic bath, at 25 °C, using a plate-plate (25 and 35 mm diameter, 1 mm gap) geometry. Small-amplitude oscillatory shear (SAOS) tests were performed inside the linear viscoelastic regime in a frequency range of 0.03–100 rad/s. At least three replicates were done on fresh samples.

Tribological measurements were carried out in a Physica MCR-501 rheometer (Anton Paar, Austria) equipped with a tribological cell, consisting of a 6.35 mm diameter steel ball that rotates on three 45°-inclined rectangular steel plates, on which the oleogel samples acting as lubricants were spread. A constant normal load and a rotational speed of 30 N and 10 min^{-1}, respectively, were applied for 10 min. Normal force and friction coefficient were calculated from the applied axial force, the friction force measured by the rheometer and ball radius according to Heyer and Läuger [54]. The time was long enough to achieve stationary values of the friction coefficient. At least five replicates were performed for each oleogel sample. The wear scars thereby produced in the steel plates were analyzed through optical microscopy using an Olympus microscope, BX51 model (Japan), from which the average diameters were determined. The data supplied here represent the mean of the three plates.

3. Results and discussion

3.1. Physicochemical properties of LSL/PVP solutions and effect on the morphology of electrospun nanostructures

Surface tension, electrical conductivity and main shear and extensional rheological parameters of LSL/PVP solutions in DMF are collected in Table 2 as a function of total polymer concentration and LSL:PVP ratio. As can be seen, surface tension data remains roughly constant at around 35–37 mN/cm, in most cases lowering the surface tension of DMF (36.96 ± 0.02 mN/cm), according to a certain well-known amphiphilic character of both lignin [55–57] and PVP [58]. However, surface tension slightly increases with total polymer concentration and LSL:PVP ratio, as similarly reported for PVP-surfactants mixtures [59], lignin-surfactant mixtures [60] and lignin derivatives [61] above a critical aggregation concentration. Electrical conductivity of PVP (LSL-free) solutions is very low (around 10-fold higher than that of pure DMF). Instead, the addition of small amounts of LSL provides a fairly good electrical conductivity to the solution, which significantly increases with LSL content. This is again due to the polar character of lignin whose complex chemical structure is composed of phenolic and aliphatic hydroxyl and carboxyl moieties and β-*O*-4′ alkyl–aryl ether-based substructures [62]. The increasing conductivity with LSL concentration suggests that these solutions are below the overlap concentration, i.e. in the semi-diluted unentangled regime, from which the conductivity begins to decrease (unpublished results) as a consequence of the reduced mobility of the entangled macromolecules.

Regarding the shear rheology, solutions with 8 and 10 wt% total concentration of LSL/PVP blends exhibited a Newtonian behavior in the shear rate range studied, with viscosity values that increase with PVP content. In fact, LSL mainly composed of aromatic monolignols forms compact structures that are not able to easily produce physical entanglements like linear polymers such as PVP, and therefore imparts low viscosity to the solutions prepared with high LSL:PVP ratios. On the contrary, LSL/PVP solutions at 15 wt%, excepting for the 90:10 LSL:PVP ratio, showed a non-Newtonian response characterized by a tendency to reach a Newtonian plateau at moderate shear rates (at around 10 s^{-1}) followed by a shear-thinning evolution, which is well-described by the Williamson model (see Fig. 2). The values of the Williamson model parameters are included in Table 2. η_0 and K values increase with PVP concentration as well as the shear-thinning character (lower m values).

The extensional rheology of LSL/PVP solutions follows the same patterns found in lignin/PEO solutions rigorously investigated by Dallmeyer and coworkers [43]. For solutions at 8 wt% total LSL/PVP concentration and that containing 10 wt% at a 10:90 LSL:PVP ratio, the extensional properties cannot be assessed since the filament breaks up immediately after imposing the stretching strain due to the low viscosity and poor elastic properties. In all the other cases, as can be observed in Fig. 3a, a linear filament thinning evolution that is characteristic of Newtonian liquids was found for the higher LSL:PVP ratios, whereas an exponential decay of the filament diameter, typical of viscoelastic

Table 1
Electrospinning input parameters applied to obtain LSL/PVP nanostructures.

Sample	Feeding flow (ml/h)	Voltage (kV)	Neddle tip-collector distance (cm)
LSL:PVP/DMF (8 wt%)	0.5–0.8	8–12	20
LSL:PVP/DMF (10 wt%)	0.8–1.5	10–12	10–15
LSL:PVP/DMF (15 wt%)	1.0–3.0	10–15	10–12

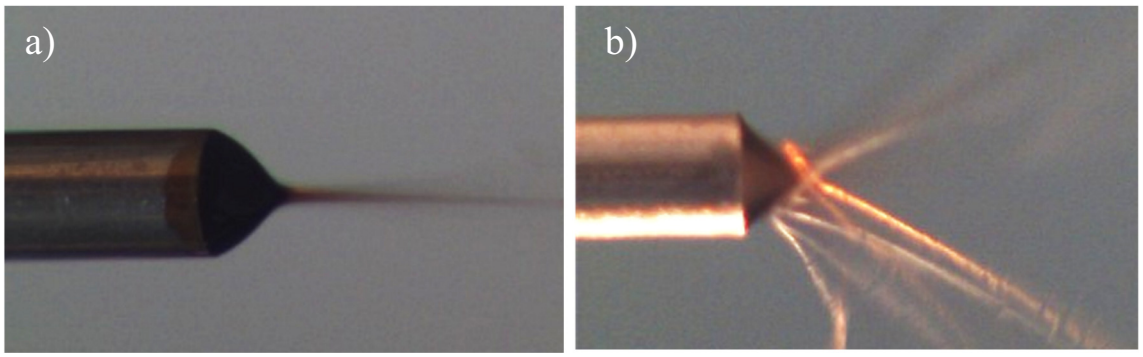

Fig. 1. a) Correct formation of the Taylor cone, and b) flow instabilities in the needle tip.

fluids, was observed for higher PVP proportions. Since capillary extensional processes are inherently transient phenomena, the apparent extensional viscosity continuously increases when moving from the coil to stretched states [63] and, as suggested by Dallmeyer and coworkers [43], a more suitable parameter to account for the whole filament thinning process is the characteristic relaxation time, λ, that can be estimated by fitting the filament thinning profiles (Fig. 3a) to:

$$\frac{D(t)}{D_o} = A\, e^{-(t/3\lambda)} = \left(\frac{G\, D_o}{4\,\sigma}\right)^{1/3} e^{-(t/3\lambda)} \quad (3)$$

where $D(t)$ is the diameter measured as a function of time in the CaBER rheometer at the filament midpoint, D_o is the initial filament diameter and G is the elastic modulus.

The characteristic relaxation times for each LSL/PVP solution are shown in Table 2 as well as the values of the fitting parameter A. Besides, since reasonably constant values of the extensional viscosity were achieved in the very short time scale (see Fig. 3b), these short time-limiting extensional viscosity values ($\eta_{ext,0}$) were also provided in Table 2. In Fig. 3b, the extensional viscosity is plotted in the form of the Trouton ratio ($Tr = \eta_{ext}/\eta_0$), showing that the theoretical value of $Tr = 3$ at low strains (or stretching times, in Fig. 3b) was reasonably accomplished, and subsequently increases with time. As expected, both the characteristic relaxation time and apparent extensional viscosity increase with total LSL/PVP concentration and decrease by increasing the LSL:PVP ratio. Significantly higher relaxation times, i.e. around one order of magnitude in most cases, were found in those solutions having a total concentration of 15 wt% in comparison to those obtained with 10 wt% solutions, coinciding with those systems for which a non-Newtonian response was found in shear flow experiments. However, as previously discussed, a certain viscoelastic character was also found in some of the solutions with 10 wt% LSL/PVP total concentrations (see Table 2), despite they displayed a Newtonian response in shear experiments.

Figs. 4 and 5 show some representative SEM images of the morphology of resulting LSL/PVP nanostructures obtained by electrospinning as a function of LSL:PVP ratio and the solution concentration, respectively. The actual LSL:PVP ratios comprising the generated electrospun nanostructures were verified experimentally by means of TGA tests, using pure lignin and PVP electrospun products as reference (see Fig. S1 and Table S1 in the Supporting information). As can be observed in Fig. 4, for a given LSL/PVP solution concentration, a transition from micro-sized particles connected by thin filaments to electrospun fiber mats was obtained by decreasing the LSL:PVP weight ratio in the solution. Moreover, it is worth noting that the diameter of the fibers increased with the PVP:LSL ratio (Fig. 4) and LSL/PVP total concentration (Fig. 5). At 15 wt% total LSL/PVP concentration and relatively high LSL:PVP ratio, i.e. 70:30, but especially at 10 wt% total concentration (see for instance Fig. 5b and e), some typical BOAS nanostructures found in lignin/PEO electrospun solutions [38,42,43] were also obtained. From solutions containing 8 wt% LSL/PVP total concentration and LSL:PVP ratios above 50:50, nanofibers were not generated but electrosprayed particles (see Fig. 5d).

Considering the physico-chemical properties of LSL/PVP solutions in DMF (Table 2) and the electrospun morphologies shown in Figs. 4 and 5, it may be inferred that the ranges of surface tension and electrical

Table 2
Electrical conductivity, surface tension and shear and extensional viscosity data of LSL/PVP solutions in DMF, as well as values of the Williamson model parameters (Eq. (1)), in the case of non-Newtonian solutions, and Eq. (3) fitting parameters, including the relaxation time in extensional filament-thinning experiments.

Concentration (wt%)	LSL:PVP ratio (%)	Electrical conductivity, Λ (μS/cm)	Surface tension, σ (mN/m)	Newtonian viscosity, μ (Pa·s)	η_o (Pa·s)	k (s)	m (−)	Extensional viscosity, $\eta_{ext,0}$ (Pa·s)	Relaxation time, λ (ms)	A (−)	D_o (mm)
	0:100	32.2 ± *0.3*	34.21 ± *0.02*	0.142 ± *0.022*	–	–	–	–	–	–	–
8	10:90	134.2 ± *0.2*	34.93 ± *0.04*	0.115 ± *0.004*	–	–	–	–	–	–	–
	30:70	206.0 ± *0.8*	35.01 ± *0.03*	0.094 ± *0.004*	–	–	–	–	–	–	–
	50:50	252.3 ± *2.5*	36.41 ± *0.02*	0.061 ± *0.002*	–	–	–	–	–	–	–
	70:30	366.7 ± *2.5*	36.30 ± *0.01*	0.039 ± *0.003*	–	–	–	–	–	–	–
	90:10	393.0 ± *0.8*	35.94 ± *0.01*	0.004 ± *0.001*	–	–	–	–	–	–	–
	0:100	33.1 ± *0.4*	35.12 ± *0.02*	0.332 ± *0.002*	–	–	–	2.33	145	0.8	2.3
10	10:90	138.7 ± *0.3*	35.20 ± *0.05*	0.287 ± *0.015*	–	–	–	1.03	65	1.9	1.7
	30:70	229.0 ± *3.1*	35.33 ± *0.01*	0.198 ± *0.008*	–	–	–	0.44	26	1.3	1.2
	50:50	271.3 ± *2.1*	36.35 ± *0.01*	0.094 ± *0.004*	–	–	–	0.40	21	1.2	1.1
	70:30	412.0 ± *2.0*	36.63 ± *0.02*	0.061 ± *0.005*	–	–	–	0.12	–	–	0.9
	90:10	441.7 ± *4.3*	36.58 ± *0.01*	0.016 ± *0.001*	–	–	–	–	–	–	–
	0:100	34.4 ± *0.3*	35.74 ± *0,01*	–	1.84	$1.3\cdot10^{-2}$	0.69	5.61	331	1.5	2.4
15	10:90	142.7 ± *0.6*	35.95 ± *0.01*	–	1.49	$1.1\cdot10^{-2}$	0.70	4.72	230	1.7	2.0
	30:70	275.7 ± *0.9*	36.50 ± *0.01*	–	1.19	$4.7\cdot10^{-3}$	0.77	2.99	208	1.6	1.9
	50:50	328.0 ± *2.1*	36.63 ± *0.01*	–	0.81	$3.1\cdot10^{-3}$	0.78	1.89	114	1.7	1.8
	70:30	470.7 ± *1.9*	36.91 ± *0.04*	–	0.45	$2.2\cdot10^{-3}$	0.93	0.92	39	2.7	1.4
	90:10	523.7 ± *4.7*	37.12 ± *0.02*	0.069 ± *0.003*	–	–	–	0.17	–	–	1.3

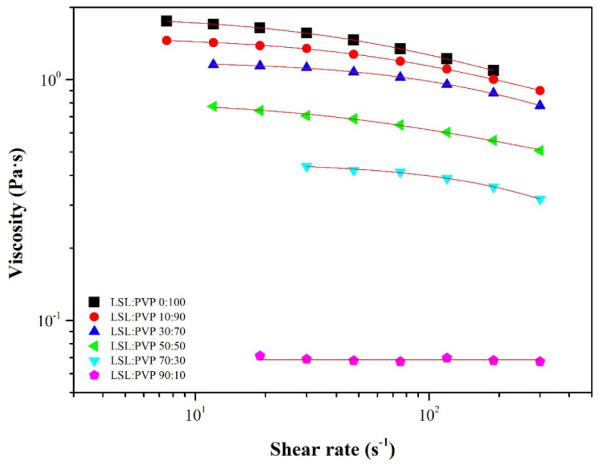

Fig. 2. Viscous flow curves of LSL/PVP solutions in DMF at 15% wt., as a function of LSL:PVP ratio and fitting to the Williamson model (Eq. (1)).

conductivity values of the solutions are, in general, suitable to obtain nanofibers and not especially relevant for tailoring a certain morphology. On the contrary, as discussed in the above referenced works, the achievement of bead-free uniform fibers, BOAS structures or just electrosprayed particles is crucially dependent on the rheological properties of the electrospun solutions. For instance, by analysing the hydrodynamic properties of sulphur-free softwood lignin/PEO solutions, Aslanzadeh et al. [38] pointed out that a certain volume fraction above that corresponding to the polymer blend overlap critical concentration is required to obtain bead-free uniform nanofibers, which is also favoured by increasing PEO/lignin ratio and PEO molecular weight. On the contrary, Dallmayer et al. [43] emphasized the role of the extensional properties of Kraft lignin/PEO solutions, which were enhanced by increasing either lignin concentration or PEO/lignin ratio, suggesting a threshold value of the characteristic relaxation time, λ, of ~12 ms for the transition from BOAS to bead-free fibers. These previous studies are in agreement with the results shown herein. In our case, relatively bead-free uniform fibers were obtained from LSL/PVP solutions having characteristic relaxation times not lower than 26 ms, and especially those exhibiting non-Newtonian behavior in shear tests, i.e. 15 wt% total concentration. Nevertheless, some Newtonian solutions with poor elastic characteristics but a certain extensional viscosity, like those having 10 wt% concentration and 70:30 LSL:PVP ratio or even 8 wt% concentration and 50:50 LSL:PVP ratio, are able to generate beaded nanofibers. On the other hand, homogeneously arranged BOAS morphologies were scarcely found. More typically, uniform nanofibers with some few beaded fibers (see Fig. 5a, b or e) or even well-developed electrospun fiber mats with embedded micro-sized particles (see Fig. 4c) were found. However, it is worth to mention that the total LSL/PVP concentrations of electrospun solutions are significantly lower than those reported in the previous literature for lignin/PEO solutions, below the critical overlap concentration as previously mentioned. For this reason, at a 90:10 LSL:PVP ratio, the Taylor cone formed during the electrospinning process is, in the best cases, relatively unstable, resulting the micro-sized particles connected by thin filaments shown in Fig. 4a, or just electrosprayed particles for the lower concentrations, i.e. 8–10 wt% (see Fig. 5d). In contrast, uniform electrospun fibers mats were generally obtained at relatively low LSL/PVP concentrations and slightly lower LSL:PVP ratios (see for instance Fig. 5e at 10 wt% total concentration and 70:30 LSL:PVP ratio). Finally, more densely distributed and thicker fibers were obtained by decreasing the LSL:PVP ratio (see Fig. 4c and d).

3.2. Oil structuring ability of LSL/PVP nanostructures

To examine the ability to form oleogels, the different electrospun LSL/PVP composite nanostructures were blended with castor oil by applying the simple methodology described in the Materials and methods section. For this study, the nanostructures obtained from 10 wt% LSL/PVP solutions were selected. As illustrated in Fig. 6a, the LSL/PVP nanostructure containing a 90:10 LSL:PVP ratio generally formed unstable dispersions, in which phase separation began to be detected immediately after blending the components. Only LSL/PVP nanostructures/castor oil blends at relatively high concentrations, i.e. 30 wt%, were physically stable against phase separation. On the contrary, nanostructures achieved with lower LSL:PVP ratios formed physically stable oleogels (see Fig. 6), with the exception of the nanostructure containing a 70:30 LSL:PVP proportion which also showed limited stability at 10 wt % concentration in castor oil, exhibiting phase separation after 24–48 h from preparation (see Fig. 6d). In general, it can be concluded that the formation of uniform bead-free fibers or beaded fibers by electrospinning is required to form physically stable oleogels, whereas electrosprayed spherical particles, or randomly distributed aggregates of particles interconnected by thin filaments, inexorably give rise to unstable dispersions. Therefore, nanofiber mats are able to entrap castor oil more favourably, thus enhancing the physical interactions between the oil and the LSL/PVP composite nanofibers. In this sense, the oleogelation mechanism seems to be very similar to that proposed for

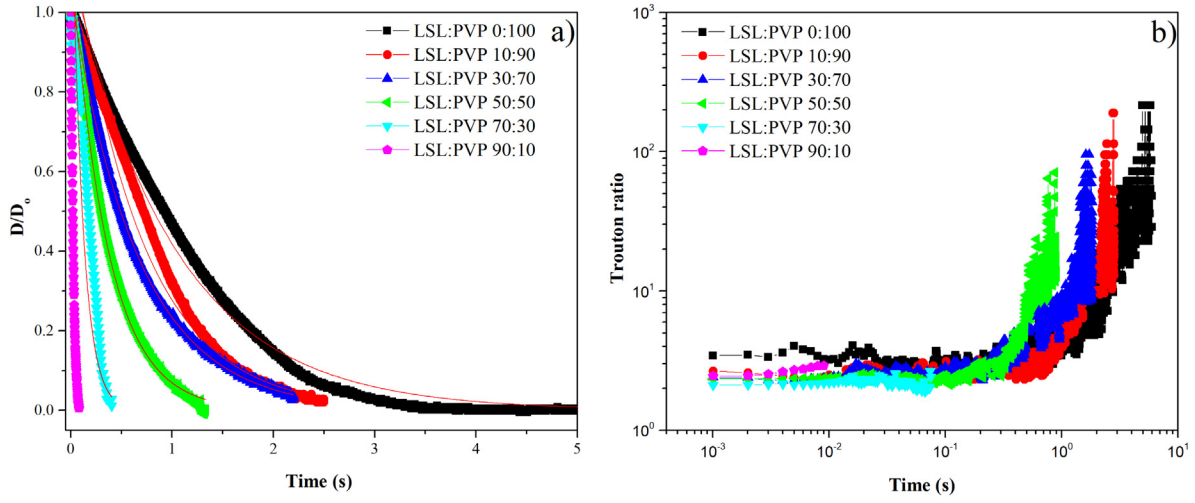

Fig. 3. Evolution of a) normalized filament diameter and b) Trouton ratio with time in the transient extensional experiments for LSL/PVP solutions in DMF at 15% wt., as a function of LSL:PVP ratio.

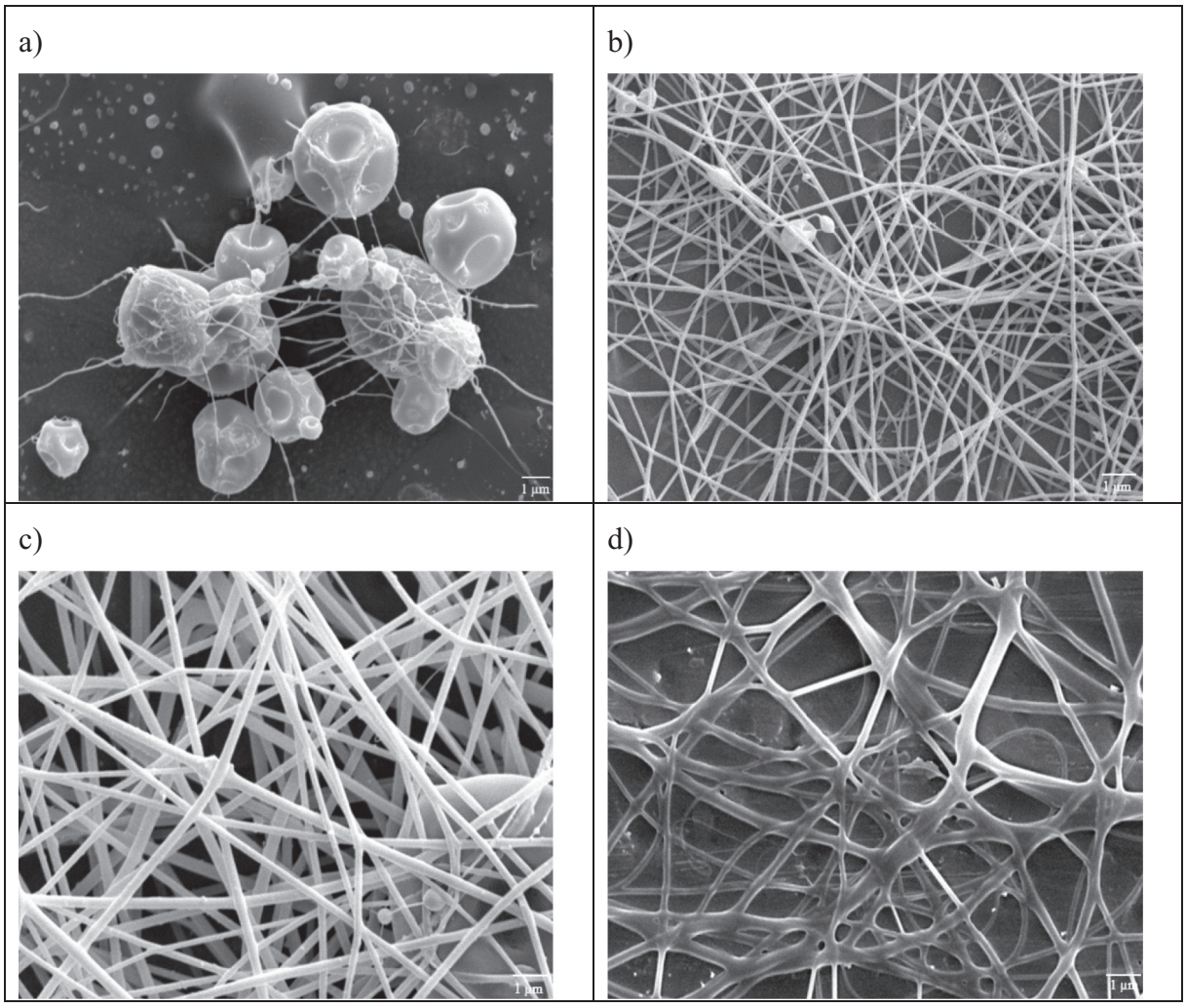

Fig. 4. SEM images of electrospun LSL/PVP nanostructures obtained from solutions in DMF at 15% wt at different LSL:PVP ratios: a) 90:10, b) 70:30, c) 50:50, and d) 30:70 (magnification x4000).

dried foam-templates [17,64] or protein freeze-dried aggregates [65], where the oil is absorbed in the generated voids by directly immersing or dispersing these templates or powders into the oil. These authors emphasized the importance of obtaining large available surface areas to achieve self-standing oleogels.

Besides, as can be seen at first glance in Fig. 6, variable oleogel consistency was obtained depending on the nanofiber LSL:PVP ratio and their concentration in castor oil. Fig. 7 shows the mechanical spectra of resulting oleogels as a function of LSL/PVP nanofiber concentration (Fig. 7a) and nanofiber LSL:PVP ratio (Fig. 7b). The evolution of the linear viscoelastic functions with frequency is, in all cases, concordant with the definition given by Almdal et al. [66] for solid-like gels, i.e. a plateau region with G' higher than G" in the whole frequency range studied. As expected, the values of both SAOS functions increased with nanofiber concentration (Fig. 7a), as typically found in other oleogels and gel-like dispersions such as lubricating greases [25,67,68]. This fact allows the consistency of the oleogel to be modulated or adjusted, within decades of G' and G" values, once the electrospun nanostructure is able to stabilize the system, as typically done in the lubricating grease industry by modifying the concentration of metallic soap thickeners to adjust the NLGI degree [69]. Moreover, the relative elasticity of the oleogel slightly increases with nanofibers content (average values of the loss tangent changing from 0.45 to 0.15 when varying concentration from 10 to 30% wt.). On the other hand, at a fixed concentration, a decrease in the nanofiber LSL:PVP ratio also produced an enhancement of oleogel strength, significantly increasing the values of the SAOS functions (see Fig. 7b). Finally, gel-like rheological properties are not greatly affected by temperature up to around 100 °C (see Fig. S2 in the Supporting information), which is also a desirable feature for a potential use as lubricating grease [70]. SAOS functions decreased with temperature in the 10–50 °C range but, unexpectedly, a certain reversible temperature-induced hardening effect was found above 50 °C, which needs to be investigated in more detail.

3.3. Tribological performance of LSL/PVP nanostructures-based oleogels

To explore a potential industrial application of these LSL/PVP nanostructures-based oleogels as bio-based lubricating grease formulations, the tribological performance was assessed in a ball-on-plates steel-steel tribological contact [54]. Table 3 collects the stationary values of the friction coefficient and the corresponding average diameter of wear scars generated during the friction experiments. In general, satisfactory values of the friction coefficient were obtained, comparable to or even lower than those obtained under similar operating conditions when conventional lithium and calcium greases [9,71], or functionalized cellulose- or lignin-based oleogels [9,10] were used as lubricants. The higher friction coefficient values were found when oleogel samples with softer rheological characteristics were used as lubricants, i.e. oleogels formed with the 90:10 LSL:PVP nanostructure at 30 wt% and 70:30 and 50:50 LSL:PVP nanofibers at 10 wt%. On the contrary, those

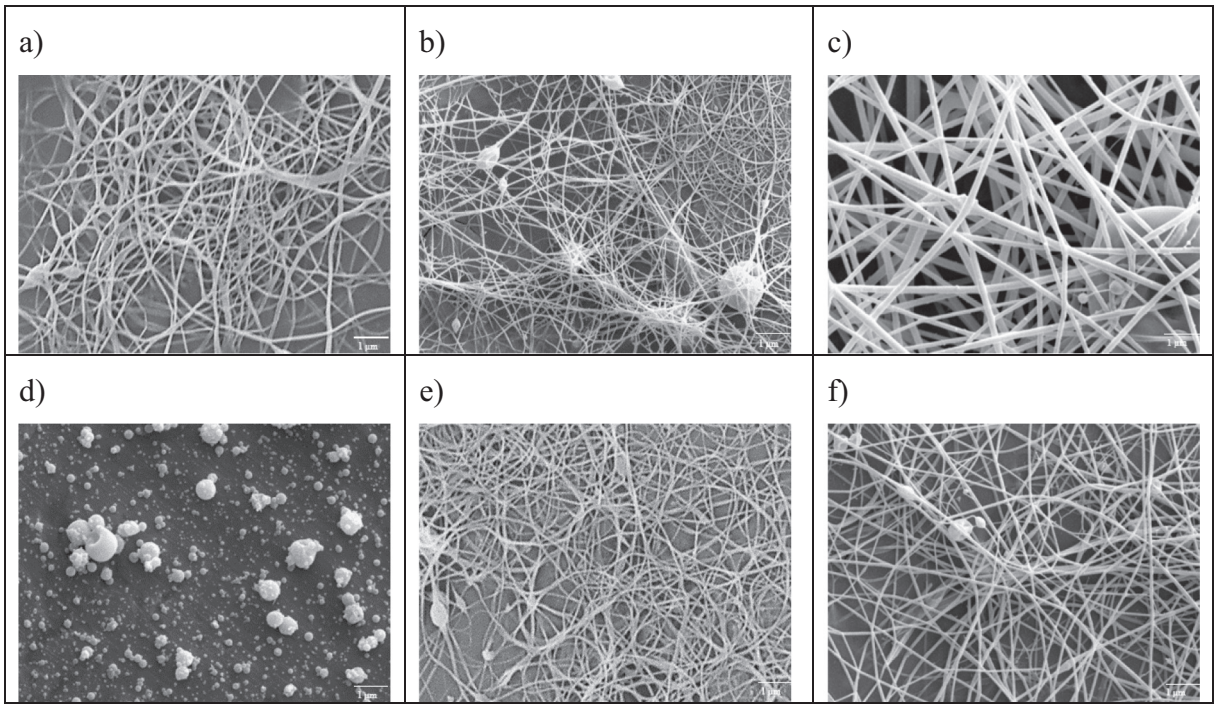

Fig. 5. SEM images of electrospun LSL/PVP nanostructures obtained from solutions having different LSL:PVP total concentration: a) 8% wt. 50:50 LSL:PVP ratio, b) 10% wt. 50:50 LSL:PVP ratio c) 15% wt. 50:50 LSL:PVP ratio, d) 8% wt. 70:30 LSL:PVP ratio, e) 10% wt. 70:30 LSL:PVP ratio and f) 15% wt. 70:30 LSL:PVP ratio (magnification x4000).

samples exhibiting enhanced gel strength significantly reduced friction, as for instance oleogels containing 30 wt% and 20 wt% of 70:30 and 50:50 LSL:PVP nanofibers, respectively. Moreover, wear was minimized or even completely prevented when using these relatively strong oleogels as lubricants in the tribological cell. For instance, not wear mark was detected by microscopy analysis for oil structured with 70:30 and 50:50 LSL:PVP nanofibers at 30 wt% and 20 wt% concentration, respectively (Table 3). In contrast, larger wear scars were generated when using softer oleogels, especially the one composed of micro-sized particles instead of nanofibers, i.e. the 90:10 LSL:PVP ratio

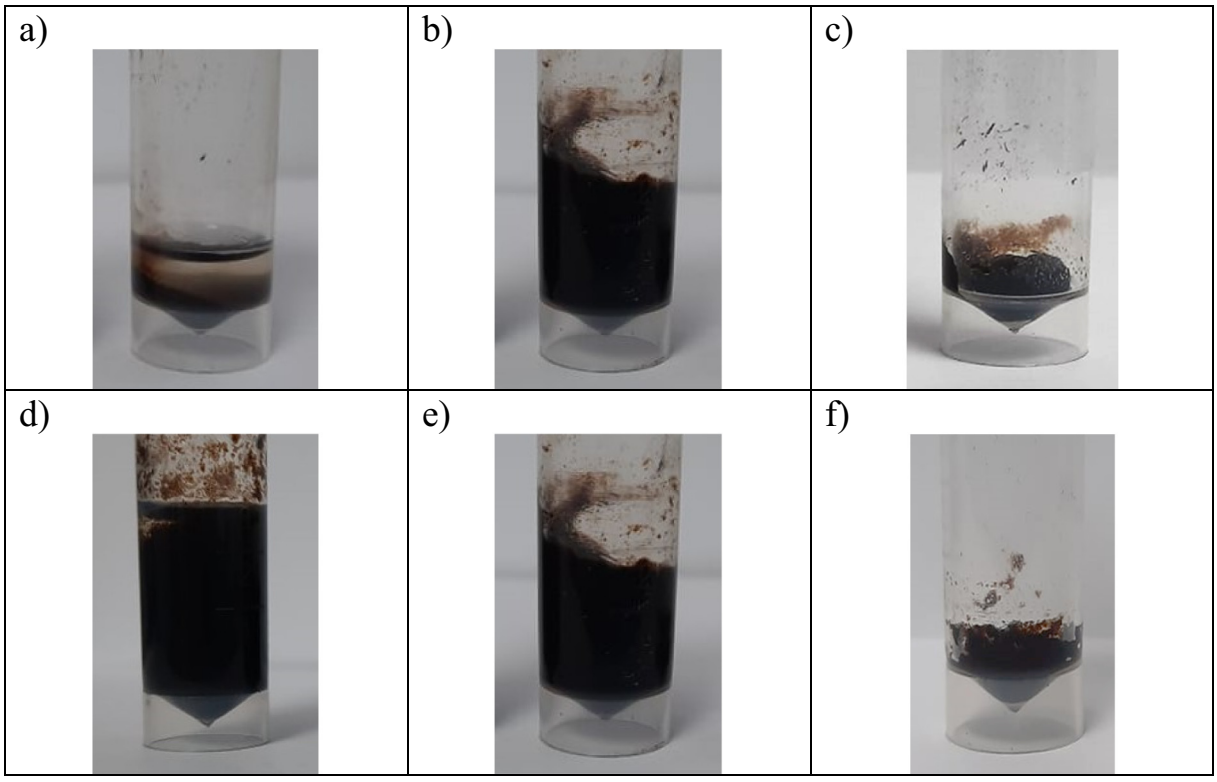

Fig. 6. Physical appearance of a-c) LSL/PVP nanostructures of different LSL:PVP ratios dispersed in castor oil at 20% wt. (a: 90:10, b: 70:30, c: 50:50), and d-f) 70:30 LSL:PVP nanostructure dispersed in castor oil at several concentrations (a: 10% wt., b: 20% wt., c: 30%).

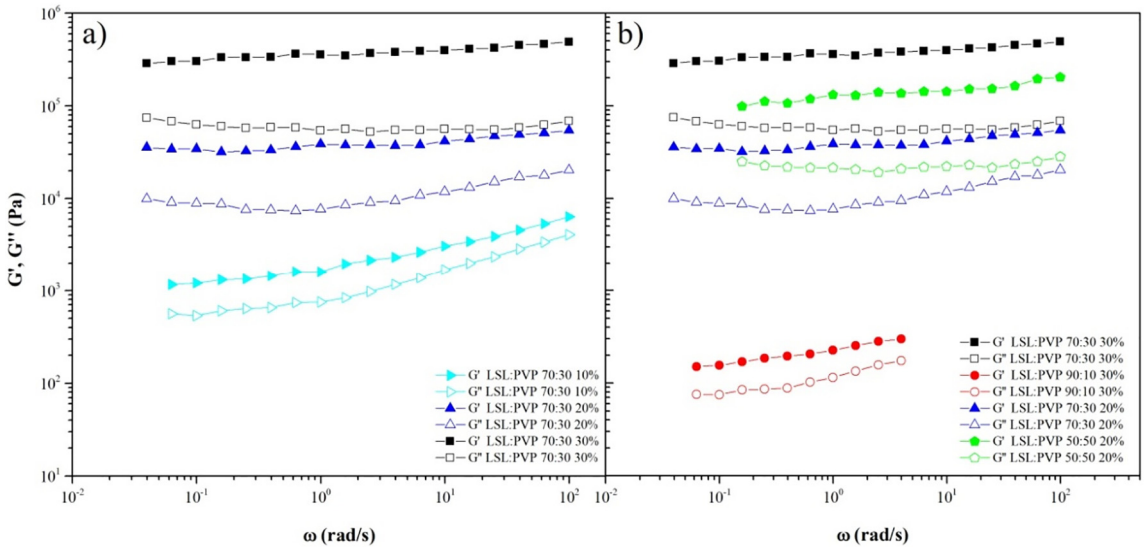

Fig. 7. Mechanical spectra (G′: filled symbols; G″: empty symbols) of electrospun LSL/PVP nanofibers-based oleogels, as a function of a) nanofiber concentration (70:30 LSL:PVP ratio) and b) LSL:PVP ratios (20 and 30% nanofiber concentration).

nanostructure (see Table 3 and Fig. S3 in the Supporting information). Since the oil medium was the same in all oleogel samples, the differences found must be attributed to the morphology of the electrospun nanostructures used as structuring agent. As above mentioned, well-developed and uniform nanofiber mats favour oil entrapment and are able to penetrate in the lubricating contact as a whole, promoting oil release only once the nanostructure is highly stressed in the contact. Instead, it can be hypothesized that the nanostructure of softer oleogels and, especially, those comprising micro-sized particles, at high LSL:PVP ratios, may have higher difficulty in penetrating into the contact but, at the same time, probably more easily release oil, which tends to enter into the contact by itself, thus reducing the lubricant film thickness and favouring friction and wear.

4. Conclusions

Different micro- and nano-structures were successfully obtained by electrospinning from low sulfonate Kraft lignin (LSL)/polyvinylpyrrolidone (PVP) solutions in DMF. In general, LSL/PVP solutions showed appropriate surface tension and electrical conductivity values for electrospinning. However, the morphology of the composite nanostructure generated is greatly affected by the rheological properties of the solution, which depends on the LSL/PVP total concentration and LSL:PVP ratio. Electrosprayed nanoparticles or micro-sized particles connected by thin filaments were obtained from solutions with low LSL/PVP concentrations and/or high LSL:PVP ratios, whereas beaded fibers and uniform fibers mats were obtained by increasing the solution concentration and/or decreasing the LSL:PVP ratio.

The formation of bead-free uniform nanofibers was favoured by using LSL/PVP solutions with certain viscoelastic characteristics in filament-thinning extensional tests, i.e. showing relaxation times of at least 26 ms, and non-Newtonian character in shear tests. The diameter of nanofibers increased with both the PVP:LSL ratio and total concentration. Regardless of the concentration, solutions with 90:10 LSL:PVP ratio were not able to generate fibers but, in the best case, micro-sized particles connected by filaments. However, uniform fibers with some few beaded fibers randomly distributed were achieved from solutions with relatively high LSL:PVP ratios or low LSL/PVP concentration, like for instance those having 10% wt. concentration and 70:30 LSL:PVP ratio or 8% wt. concentration and 50:50 LSL:PVP ratio.

Generated electrospun LSL/PVP fiber mats were able to form stable oleogels simply by dispersing them into the castor oil at concentrations between 10 and 30 wt%. The formation of, at least, beaded fibers was required to physically stabilize the oleogels. Instead, the micro-sized particles connected by filaments generally gave rise to unstable dispersions. The rheological properties of the oleogels may be tailored by modifying the LSL:PVP ratio, according to the morphology of the nanofiber network, and nanofiber concentration. These oleogels also demonstrated remarkable tribological performance to be potentially applied as bio-based lubricating greases. Overall, electrospinning of lignin/PVP solutions can be proposed as a simple and effective method to produce micro- and nano-architectures for oil structuring purposes, resulting in oleogels with potential applications in different fields, such as in the lubricant industry.

Table 3
Values of the friction coefficient and wear scar average diameter obtained in a tribological cell when using the electrospun LSL/PVP nanofibers-based oleogels as lubricants.

LSL:PVP ratio (wt%)	Concentration of LSL/PVP nanostructures (wt%)	Friction coefficient (−)	Wear scar diameter (μm)
50:50	20	0.049 ± *0.003*	–
	10	0.208 ± *0.015*	361 ± *37*
70:30	30	0.054 ± *0.005*	–
	20	0.093 ± *0.010*	346 ± *46*
	10	0.135 ± *0.006*	362 ± *53*
90:10	30	0.176 ± *0.056*	959 ± *81*

CRediT authorship contribution statement

M. Borrego: Investigation, Data Curation, Validation, Formal analysis.
J.E. Martín-Alfonso: Conceptualization, Methodology, Formal analysis, Investigation, Supervision.
M.C. Sánchez: Investigation, Formal analysis, Supervision.
C. Valencia: Investigation, Supervision, Funding acquisition.
José M. Franco: Conceptualization, Methodology, Investigation, Formal analysis, Writing - original draft, Writing - review & editing, Supervision, Project administration, Funding acquisition.

Acknowledgements

This work is part of a research project (RTI2018-096080-B-C21) sponsored by the MICINN-FEDER I+D+i Spanish Programme. The financial support is gratefully acknowledged.

Appendix A. Supplementary data

Supplementary data to this article can be found online at https://doi.org/10.1016/j.ijbiomac.2021.03.069.

References

[1] C.M. O'Sullivan, S. Barbut, A.G. Marangoni, Edible oleogels for the oral delivery of lipid soluble molecules: composition and structural design considerations, Trends Food Sci. Technol. 57 (2016) 59–73.
[2] A.R. Patel, Colloidal gel perspective for understanding oleogelation, Curr. Opin. Food Sci. 15 (2017) 1–7.
[3] A.R. Patel, Structuring edible oils with hydrocolloids: where do we stand? Food Biophys 13 (2018) 113–115.
[4] C. Park, F. Maleky, C. Park, F. Maleky, A critical review of the last 10 years of oleogels in food, Front. Sustain. Food Syst. 4 (2020) 139.
[5] S. Pakseresht, M.M. Tehrani, Advances in multi-component supramolecular oleogels - a review, Food Rev. Int. (2020)https://doi.org/10.1080/87559129.2020.1742153 published online.
[6] M. Davidovich-Pinhas, Oleogels: a promising tool for delivery of hydrophobic bioactive molecules, Ther. Deliv. 7 (2016) 1–3.
[7] R. Macoon, A. Chauhan, Dispersion of drug particles and emulsion drops in oleogels for ophthalmic drug delivery, Abstr. Pap. Am. Chem. Soc. 258 (2019), 22-IEC, .
[8] D. Ash, S.B. Majee, G.R. Biswas, Span 40/tween 80-based soybean oleogels: modeling of gelation kinetics and drug release, Int. J. Pharm. Sci. Res. 10 (2019) 4538–4545.
[9] R. Gallego, M.T. Cidade, R. Sánchez, C. Valencia, J.M. Franco, Tribological behaviour of novel chemically modified biopolymer-thickened lubricating greases investigated in a steel-steel rotating ball-on-three plates tribology cell, Tribol. Int. 94 (2016) 652–660.
[10] M.A. Delgado, E. Cortes-Triviño, C. Valencia, J.M. Franco, Tribological study of epoxide-functionalized alkali lignin-based gel-like biogreases, Tribol. Int. 146 (2020), 106231.
[11] K. Gao, Q.Y. Chang, B. Wang, The dispersion and tribological performances of magnesium silicate hydroxide nanoparticles enhanced by Span60 oleogel, J. Sol-Gel Sci. Technol. (1) (2020) 165–173.
[12] M. Suzuki, K. Hanabusa, Polymer organogelators that make supramolecular organogels through physical cross-linking and self-assembly, Chem. Soc. Rev. 39 (2010) 455–463.
[13] J.E. Martín-Alfonso, N. Núñez, C. Valencia, J.M. Franco, M.J. Díaz, Formulation of new biodegradable lubricating greases using ethylated cellulose pulp as thickener agent, J. Ind. Eng. Chem. 17 (2011) 818–823.
[14] M. Davidovich-Pinhas, S. Barbut, A.G. Marangoni, The gelation of oil using ethyl cellulose, Carbohydr. Polym. 117 (2015) 869e878.
[15] A.K. Zetzl, A.J. Gravelle, M. Kurylowicz, J. Dutcher, S. Barbut, A.G. Marangoni, Microstructure of ethylcellulose oleogels and its relationship to mechanical properties, Food Struct. 2 (2014) 27–40.
[16] A.J. Gravelle, A.G. Marangoni, Ethylcellulose oleogels: structure, functionality, and food applications, Adv. Food Nutr. Res. 84 (2018) 1–56.
[17] A.R. Patel, D. Schatteman, A. Lesaffer, K. Dewettinck, A foam-templated approach for fabricating organogels using a water-soluble polymer, RSC Adv. 3 (2013) 22900–22903.
[18] A.R. Patel, N. Cludts, M.D.B. Sintang, B. Lewille, A. Lesaffer, K. Dewettinck, Polysaccharide-based oleogels prepared with an emulsion-templated approach, ChemPhysChem 15 (2014) 3435–3439.
[19] W. Wijaya, P. Van der Meeren, K. Dewettinck, A.R. Patel, High internal phase emulsion (HIPE)-templated biopolymeric oleofilms containing an ultra-high concentration of edible liquid oil, Food Funct. 9 (2018) 1993–1997.
[20] A. de Vries, J. Hendriks, E. van der Linden, E. Scholten, Protein oleogels from protein hydrogels via a stepwise solvent exchange route, Langmuir 31 (2015) 13850–13859.
[21] A. de Vries, A. Wesseling, E. van der Linden, E. Scholten, Protein oleogels from heat-set whey protein aggregates, J. Colloid Interface Sci. 486 (2017) 75–83.
[22] J.E. Martin-Alfonso, R. Yañez, C. Valencia, J.M. Franco, M.J. Díaz, Optimization of the methylation conditions of kraft cellulose pulp for its use as a thickener agent in biodegradable lubricating greases, Ind. Eng. Chem. Res. 48 (2009) 6765–6771.
[23] R. Sánchez, G.B. Stringari, J.M. Franco, C. Valencia, C. Gallegos, Use of chitin, chitosan and acylated derivatives as thickener agents of vegetable oils for bio-lubricant applications, Carbohydr. Polym. 85 (2011) 705–714.
[24] R. Sánchez, G. Alonso, C. Valencia, J.M. Franco, Rheological and TGA study of acylated chitosan gel-like dispersions in castor oil: influence of acyl substituent and acylation protocol, Chem. Eng. Res. Des. 100 (2015) 170–178.
[25] R. Gallego, J.F. Arteaga, C. Valencia, J.M. Franco, Rheology and thermal degradation of isocyanate-functionalized methyl cellulose-based oleogels, Carbohydr. Polym. 98 (2013) 152–160.
[26] R. Gallego, J.F. Arteaga, C. Valencia, J.M. Franco, Thickening properties of several NCO-functionalized cellulose derivatives in castor oil, Chem. Eng. Sci. 134 (2015) 260–268.
[27] R. Gallego, J.F. Arteaga, C. Valencia, M.J. Díaz, J.M. Franco, Gel-like dispersions of hmdi-cross-linked lignocellulosic materials in castor oil: toward completely renewable lubricating grease formulations, ACS Sustain. Chem. Eng. 3 (2015) 2130–2141.
[28] E. Cortés-Triviño, C. Valencia, J.M. Franco, Influence of epoxidation conditions on the rheological properties of gel-like dispersions of epoxidized kraft lignin in castor oil, Holzforschung 71 (2017) 777–784.
[29] E. Cortés-Triviño, C. Valencia, M.A. Delgado, J.M. Franco, Rheology of epoxidized cellulose pulp gel-like dispersions in castor oil: influence of epoxidation degree and the epoxide chemical structure, Carbohydr. Polym. 199 (2018) 563–571.
[30] A.M. Borrero-López, C. Valencia, J.M. Franco, Rheology of lignin-based chemical oleogels prepared using diisocyanate crosslinkers: effect of the diisocyanate and curing kinetics, Eur. Polym. J. 89 (2017) 311–323.
[31] D. Muller, C. Matta, R. Thijssen, M.N. bin Yusof, M.C.P. van Eijk, S. Chatra, Novel polymer grease microstructure and its proposed lubrication mechanism in rolling/sliding contacts, Tribol. Int. 110 (2017) 278–290.
[32] S. Octave, D. Thomas, Biorefinery: toward an industrial metabolism, Biochimie 91 (2009) 659–664.
[33] A.J. Ragauskas, G.T. Beckham, M.J. Biddy, R. Chandra, F. Chen, M.F. Davis, B.H. Davison, R.A. Dixon, P. Gilna, M. Keller, P. Langan, A.K. Naskar, J.N. Saddler, T.J. Tschaplinski, G.A. Tuskan, C.E. Wyman, Lignin valorization: improving lignin processing in the biorefinery, Science 344 (2014), 1246843.
[34] S. Laurichesse, L. Avérous, Chemical modification of lignins: towards biobased polymers, Prog. Polym. Sci. 39 (2014) 1266–1290.
[35] Z. Chen, X. Mo, F. Qing, Electrospinning of collagen–chitosan complex, Mater. Lett. 61 (2007) 3490–3494.
[36] N. Bhardwaj, S.C. Kundu, Electrospinning: a fascinating fiber fabrication technique, Biotech. Adv. 28 (2010) 325–347.
[37] D.K. Shu, P. Xi, B.W. Cheng, Y. Wang, L. Yang, X.Q. Wang, X.H. Yan, One-step electrospinning cellulose nanofibers with superhydrophilicity and superoleophobicity underwater for high-efficiency oil-water separation, Int. J. Biol. Macromol. 162 (2020) 1536–1545.
[38] S. Aslanzadeh, B. Ahvazi, Y. Boluk, C. Ayranci, Morphologies of electrospun fibers of lignin in poly(ethylene oxide)/N,N dimethylformamide, J. Appl. Polym. Sci. 133 (2016) 44172.
[39] A. Duval, M. Lawoko, A review on lignin-based polymeric, micro- and nano-structured materials, React. Funct. Polym. 85 (2014) 78–96.
[40] D. Kai, W. Ren, L. Tian, P. Lin Chee, Y. Liu, S. Ramakrishna, X.J. Loh, Engineering poly (lactide)-lignin nanofibers with antioxidant activity for biomedical application, ACS Sust. Chem. Eng. 4 (2016) 5268–5276.
[41] J. Wang, L. Tian, B. Luo, S. Ramakrishna, D. Kai, X.J. Loh, I.H. Yang, G.R. Deen, X. Mo, Engineering PCL/lignin nanofibers as an antioxidant scaffold for the growth of neuron and Schwann cell, Colloid Surf. B 169 (2018) 356–365.
[42] I. Dallmeyer, F. Ko, J.F. Kadla, Electrospinning of technical lignins for the production of fibrous networks, J. Wood Chem. Technol. 30 (2010) 315–329.
[43] I. Dallmeyer, F. Ko, J.F. Kadla, Correlation of elongational fluid properties to fiber diameter in electrospinning of softwood kraft lignin solutions, Ind. Eng. Chem. Res. 53 (2014) 2697–2705.
[44] C. Lai, Z. Zhou, L. Zhang, X. Wang, Q. Zhou, Y. Zhao, Y. Wang, X.F. Wu, Z. Zhu, H. Fong, Free-standing and mechanically flexible mats consisting of electrospun carbon nanofibers made from a natural product of alkali lignin as binder-free electrodes for high-performance supercapacitors, J. Power Sourc. 247 (2014) 134–141.
[45] M. Ago, K. Okajima, J.E. Jakes, S. Park, O.J. Rojas, Lignin-based electrospun nanofibers reinforced with cellulose nanocrystals, Biomacromolecules 13 (2012) 918–926.
[46] G. Gao, I. Dallmeyer, J.F. Kadla, Synthesis of lignin nanofibers with ionic-responsive shells: water-expandable lignin-based nanofibrous mats, Biomacromolecules 13 (2012) 3602–3610.
[47] D. Kai, H.M. Chong, L.P. Chow, L. Jiang, Q. Lin, K. Zhang, H. Zhang, Z. Zhang, X.J. Loh, Strong and biocompatible lignin/poly (3-hydroxybutyrate) composite nanofibers, Comp. Sci. Technol. 158 (2018) 26–33.
[48] D. Kai, K. Zhang, L. Jiang, Z.H. Wong, Z. Li, Z. Zhang, X.J. Loh, Sustainable and antioxidant lignin-polyester copolymers and nanofibers for potential healthcare applications, ACS Sust. Chem. Eng. 5 (2017) 6016–6025.
[49] M.S.N. Oliveira, R. Yeh, G.H. McKinley, Iterated stretching, extensional rheology and formation of beads-on-a-string structures in polymer solutions, J. Non-Newtonian Fluid Mech. 137 (2006) 137–148.
[50] L.A. Quinchia, M.A. Delgado, C. Valencia, J.M. Franco, C. Gallegos, Viscosity modification of different vegetable oils with EVA copolymer for lubricant applications, Ind. Crop. Prod. 32 (2010) 607–612.
[51] V. Sharma, S.J. Haward, J. Serdy, B. Keshavarz, A. Soderlund, P. Threlfall-Holmes, G.H. McKinley, The rheology of aqueous solutions of ethyl hydroxy-ethyl cellulose (EHEC) and its hydrophobically modified analogue (hmEHEC): extensional flow response in capillary break-up, jetting (ROJER) and in a cross-slot extensional rheometer, Soft Matter 11 (2015) 3251–3270.
[52] W. Mathues, S. Formenti, C. McIlroy, O.G. Harlen, C. Clasen, CaBER vs ROJER-different time scales for the thinning of a weakly elastic jet, J. Rheol. 62 (2018) 1135–1153.
[53] O. Arnolds, H. Buggisch, D. Sachsenheimer, N. Willenbacher, Capillary breakup extensional rheometry (CaBER) on semi-dilute and concentrated polyethyleneoxide (PEO) solutions, Rheol. Acta 49 (2010) 1207–1217.
[54] P. Heyer, J. Läuger, Correlation between friction and flow of lubricating greases in a new tribometer device, Lubr. Sci. 21 (2009) 253–268.
[55] S. Li, D. Ogunkoyac, T. Fang, J. Willoughby, O.J. Rojas, Carboxymethylated lignins with low surface tension toward low viscosity and highly stable emulsions of crude bitumen and refined oils, J. Colloid Interface Sci. 482 (2016) 27–38.
[56] M. Azadfar, W.C. Hiscox, S. Chen, Solubilization of lignin in copolymer micelles in aqueous solution, Colloids Surf. A Physicochem. Eng. Asp. 503 (2016) 1–10.
[57] T.M. Budnyak, A. Slabon, M.H. Sipponen, Lignin-inorganic interfaces: chemistry and applications from adsorbents to catalysts and energy storage materials, Chem. Sus. Chem. 13 (2020) 4344–4355.
[58] F. Yañez, A. Concheiro, C. Alvarez-Lorenzo, Macromolecule release and smoothness of semi-interpenetrating PVP–pHEMA networks for comfortable soft contact lenses, Eur. J. Pharm. Biopharm. 69 (2008) 1094–1103.

[59] C. Hu, Z. Du, X. Tai, X. Liu, Study on the interactions between SDBS/SOE-60 mixed surfactant and PVP in solution, J. Appl. Polym. Sci. 135 (2018), 46717.
[60] C. Mao, S. Wu, Solubilization of lignin in copolymer micelles in aqueous solution, Bioresources 8 (2013) 5025–5035.
[61] N. Alwadani, N. Ghavidel, P. Fatehi, Surface and interface characteristics of hydrophobic lignin derivatives in solvents and films, Colloids Surf. A Physicochem. Eng. Asp. 609 (2021), 125656.
[62] A.M. Borrero-López, R. Martin-Sampedro, D. Ibarra, C. Valencia, M.E. Eugenio, J.M. Franco, Evaluation of lignin-enriched side-streams from different biomass conversion processes as thickeners in bio-lubricant formulations, Int. J. Biol. Macromol. 162 (2020) 1398–1413.
[63] S.L. Anna, G.H. McKinley, D.A. Nguyen, T. Sridhar, S.J. Muller, J. Huang, D.F. James, An interlaboratory comparison of measurements from filament-stretching rheometers using common test fluids, J. Rheol. 45 (2001) 83–114.
[64] M. Abdollahi, S.A.H. Goli, N. Soltanizadeh, Physicochemical properties of foam-templated oleogel based on gelatin and xanthan gum, Eur. J. Lipid Sci. Technol. 122 (2020), 1900196.
[65] A. de Vries, Y. Lopez Gomez, B. Jansen, E. van der Linden, E. Scholten, Controlling agglomeration of protein aggregates for structure formation in liquid oil: a sticky business, ACS Appl. Mater. Interfaces 9 (2017) 10136–10147.
[66] K. Almdal, J. Dyre, S. Hvidt, O. Kramer, Towards a phenomenological definition of the term "gel", Polym. Gels Net. 1 (1993) 5–17.
[67] M.A. Delgado, C. Valencia, M.C. Sanchez, J.M. Franco, C. Gallegos, Influence of soap concentration and oil viscosity on the rheology and microstructure of lubricating greases, Ind. Eng. Chem. Res. 45 (2006) 1902–1910.
[68] J.E. Martín-Alfonso, G. Moreno, C. Valencia, M.C. Sánchez, J.M. Franco, C. Gallegos, Influence of soap/polymer concentration ratio on the rheological properties of lithium lubricating greases modified with virgin LDPE, J. Ind. Eng. Chem. 15 (2009) 687–693.
[69] NLGI, Lubricating Greases Guide, 5th ed., 2006 (Kansas City).
[70] M.A. Delgado, C. Valencia, M.C. Sanchez, J.M. Franco, C. Gallegos, Thermorheological behaviour of a lithium lubricating grease, Tribol. Lett. 23 (2006) 47–54.
[71] R. Sánchez, C. Valencia, J.M. Franco, Rheological and tribological characterization of a new acylated chitosan-based biodegradable lubricating grease: a comparative study with traditional lithium and calcium greases, Tribol. Trans. 57 (2014) 445–454.